Conical Diffraction in Honeycomb lattices

Mark J. Ablowitz, Sean D. Nixon, and Yi Zhu*
Department of Applied Mathematics, University of Colorado, 526 UCB, Boulder, CO 80309-0526

(Dated: March 15, 2009)

Conical diffraction in honeycomb lattices is analyzed. This phenomena arises in nonlinear Schrödinger (NLS) equations with honeycomb lattice potentials. In the tight binding approximation the wave envelope is governed by a nonlinear Dirac equation. Numerical simulations show that the Dirac equation and the lattice equation have the same conical diffraction properties. Similar conical diffraction occurs in both the linear and nonlinear regimes. The Dirac system reveals the underlying mechanism for the existence of conical diffraction in honeycomb lattices.

PACS numbers:

Conical diffraction is a fundamental feature of crystal optics and is of interest in mathematics and physics. Conical diffraction is the mechanism under which a narrow beam entering a biaxial crystal along its optic axis spreads into a hollow cone within the crystal. This phenomenon was first predicted by W. Hamilton [1] in 1832 and observed by H. Lloyd [2] soon afterwards. It has been studied experimentally and theoretically over the years (see the important article by M. Berry and M. Jeffrey [3]). A key property associated with conical diffraction is the existence of so-called diabolical points where two different dispersion surfaces touch each other. Interestingly the conical diffraction phenomenon also exists in the light beam propagation in honeycomb lattices as shown in recent work both experimentally and numerically [7, 9].

It is well-known that the material graphene has honeycomb lattice structure. In the graphene literature, it has been shown that two different energy bands can touch each other at certain isolated points which are called Dirac points; i.e. such Dirac points are diabolical points. Thus diabolical points also exist in the band structure of two-dimensional honeycomb lattices. Moreover the structure of the dispersion relation near these Dirac points are conical in nature [5, 6]; the regions in the neighborhood of Dirac points are called Dirac cones.

Like optics, Bose-Einstein condensation (BEC) can have lattice backgrounds and they both are governed by lattice NLS equations. Recently, a nonlinear Dirac equation describing a weakly interacting bosonic gas in the presence of a honeycomb optical lattice for BEC [4] was derived. The Dirac points in BEC are thus diabolical points.

In this paper we derive the evolution equations for the wave envelope of the Bloch modes in the vicinity of diabolical points directly from the lattice nonlinear Schrödinger equation; a similar derivation can also be employed on the nonlinear optical Helmholtz equation. It turns out that the governing equation is nonlinear

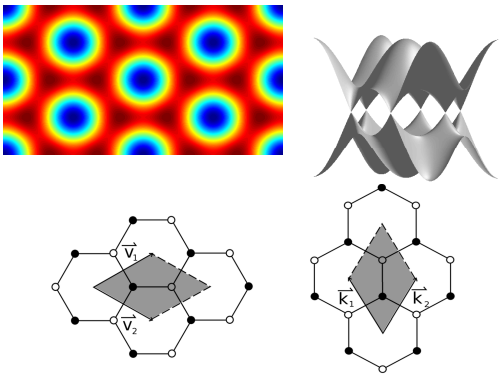

FIG. 1: The honeycomb lattice (top left) and its first two bands (top right). The physical and reciprocal lattice are depicted (top left and right respectively). Shadow regions in the lattice and reciprocal lattice are the unit cell Ω and Brillouin zone Ω'.

Dirac system, consistent with the derivation via Hamiltonian methods in graphene and BEC ([5, 6],[4]). The linear part of the Dirac system yields a dispersion relation which is the same as that obtained from the two-dimensional wave equation; this is the same dispersion relation as that of crystal optics [3] and helps explain why the beam propagates in a conical manner. This is further supported by simulations of the Dirac and lattice NLS equations and it is found that the same conical diffraction phenomena occurs in both systems. Thus we associate the conical diffraction phenomena in honeycomb lattices with Dirac type systems. In fact we find conical diffraction in both the linear and nonlinear Dirac system.

The governing equation for a light beam propagating in a 2-D lattice is the lattice nonlinear Schrödinger equation

$$i\psi_z + \nabla^2\psi - V(\mathbf{r})\psi + \sigma|\psi|^2\psi = 0. \qquad (1)$$

Here σ, the coefficient of nonlinear term, is positive for focusing nonlinearity and negative for defocusing nonlinearity; $V(\mathbf{r})$ is the 2-D periodic potential and $\mathbf{r} = (x, y)$. In photonic lattices, a model which has also been widely

*Yi.Zhu@colorado.edu

used is the saturable lattice NLS equation (cf. [8]). While the analysis on the lattice NLS equation below employs a linear potential and cubic nonlinearity, it can be readily extended to a saturable-type potential term.

The potential $V(\mathbf{r})$ we study is a honeycomb lattice. In this lattice, the local minima which we call sites form hexagons. The hexagonal lattice is usually generated by interacting three plane waves. We take the following lattice potential as our prototype

$$V(\mathbf{r}) = V_0 \left| e^{ik_0 \mathbf{b}_1 \cdot \mathbf{r}} + e^{ik_0 \mathbf{b}_2 \cdot \mathbf{r}} + e^{ik_0 \mathbf{b}_3 \cdot \mathbf{r}} \right|^2; \qquad (2)$$

where $\mathbf{b}_1 = (0, 1)$, $\mathbf{b}_2 = (-\frac{\sqrt{3}}{2}, -\frac{1}{2})$ and $\mathbf{b}_3 = (\frac{\sqrt{3}}{2}, -\frac{1}{2})$; $V_0 > 0$ is the lattice intensity. This $V(\mathbf{r})$ is a honeycomb lattice with intensity minima at the hexagonal vertices. The lattice has two periods (lattice vectors)

$$\mathbf{v}_1 = \sqrt{3}a \left(\frac{\sqrt{3}}{2}, \frac{1}{2} \right), \qquad \mathbf{v}_2 = \sqrt{3}a \left(\frac{\sqrt{3}}{2}, -\frac{1}{2} \right); \quad (3)$$

where $a = \frac{4\pi}{\sqrt{3}k_0}$ is the lattice constant which is the distance of two nearest minima. The unit cell Ω is the parallelogram with $\mathbf{v}_1$ and $\mathbf{v}_2$ as its two sides(cf. Fig. 1).

The band structure of this honeycomb lattice can be obtained from the linear lattice equation; i.e. equation (1) omitting the nonlinear term

$$i\phi_z + \nabla^2 \phi - V(\mathbf{r})\phi = 0. \qquad (4)$$

The Bloch modes follow from $\phi = e^{-i\mu z} u(\mathbf{r})$; substituting this into the equation (4) one finds the eigen problem

$$\mu u + \nabla^2 u - V(\mathbf{r}) u = 0. \qquad (5)$$

It is well-known that the Bloch mode has the form $u(\mathbf{r}; \mathbf{k}) = e^{i\mathbf{k}\cdot\mathbf{r}} U(\mathbf{r}; \mathbf{k})$ where $U(\mathbf{r}; \mathbf{k})$ has the same periodicity as the potential $V(\mathbf{r})$; $\mathbf{k} = (k_x, k_y)$ is the wave number and the dispersion surface $\mu(\mathbf{k})$ has two periods

$$\mathbf{k}_1 = \frac{4\pi}{3a} \left(\frac{1}{2}, \frac{\sqrt{3}}{2} \right), \qquad \mathbf{k}_2 = \frac{4\pi}{3a} \left(\frac{1}{2}, -\frac{\sqrt{3}}{2} \right). \qquad (6)$$

$\mathbf{k}_1$ and $\mathbf{k}_2$ are referred to as the reciprocal lattice vectors which describe the Brillouin zone Ω'. $u(\mathbf{r}; \mathbf{k})$ is also periodic with respect to $\mathbf{k}$.

The eigen problem (5) can be solved numerically; this determines the dispersion relation (band structure). Typical bands 1 and 2 are displayed in Fig. 1(top right). It is seen that the first and second bands touch each other at certain isolated points and these so-called diabolical points also display a honeycomb structure in $\mathbf{k}$ plane. From Bloch theorem it follows that these diabolical points are actually the reciprocal lattice corresponding to the original potential lattice.

There are two minima in a cell for the honeycomb lattice which we use A and B to denote. All A sits or B sites differ spatially with the multiples of $\mathbf{v}_1$ and $\mathbf{v}_2$. All A sites and B sits form two different triangular lattices: A sublattice and B sublattice. In the reciprocal lattice, there are also two diabolical points in the first Brillouin zone which we call K and K'. They are depicted in Fig. 1 (bottom right). All dots are equivalent to K while all circles are equivalent to K'. For the potential (2), $K = (0, \frac{4\pi}{\sqrt{3}a})$ and $K' = (0, \frac{8\pi}{\sqrt{3}a})$.

We begin by studying the wave propagation in the honeycomb lattice numerically in equation (1). In order to understand the essential aspects of conical diffraction which has been observed to be a linear phenomenon, we first study the linear regime, i.e. $\sigma = 0$. Later we will discuss results for the nonlinear regime, $\sigma = 1$. In our simulations, $V_0 = 100$, $a = \frac{\pi}{8}$. We simulate the propagation of a wave envelope of Bloch modes near the diabolical point K. One can obtain the Bloch modes numerically and multiply the modes by a wide Gaussian envelope and use this wave packet as the initial beam. Alternatively, one can use one or more plane waves to excite the Bloch modes which is also experimentally accessible (see [7, 9]). In order to compare with this previous work, here we only display the results with the second method. The simulations with both methods are consistent. We use two initial input beams. The first one is a Gaussian envelope multiplied by the sum of two plane waves for which the $\mathbf{k}$ vectors are two opposite diabolical points K and K'. The evolution is displayed in Fig. 2 (a)-(c). It is seen that an initial bell shape structure transforms into a ring structure after some distance. The ring structures contains two bright rings. The outer one is higher than the inner one. Between two bright rings is a dark ring. This dark ring is called Poggendorff's dark ring [3]. The second initial beam is a Gaussian envelope multiplied by one plane wave of which the $\mathbf{k}$ vector is the diabolical point K. The results are displayed in Fig. 2 (d)-(f). The patterns are similar–a spot becomes two bright rings. However, the rings in the second simulation are not complete rings; they have notches at the bottom. The ring structures with notches are termed "half-turn of polarization around the ring" and which was also predicted by Hamilton and observed by Lloyd [3]. In both cases, the rings expand radially, but the width of the ring remains the same under propagation with decreasing intensity. As a result, one can see a cone in the lattice. This is exactly the so-called conical diffraction.

Next, we derive the governing equation for the propagation of the Bloch-mode envelopes. The Bloch mode $u(\mathbf{r}; \mathbf{k}) = e^{i\mathbf{k}\cdot\mathbf{r}} U(\mathbf{r}; \mathbf{k})$. is periodic with respect to $\mathbf{k}$, so it can be expanded as a Fourier series

$$u(\mathbf{r}; \mathbf{k}) = \sum_{m,n} w_{m,n}(\mathbf{r}) e^{-im\mathbf{k}\cdot\mathbf{v}_1 - in\mathbf{k}\cdot\mathbf{v}_2}. \qquad (7)$$

where $w_{m,n}(\mathbf{r}) = \frac{1}{|\Omega'|} \int_{\Omega'} u(\mathbf{r}; \mathbf{k}) e^{-im\mathbf{k}\cdot\mathbf{v}_1 - in\mathbf{k}\cdot\mathbf{v}_2} d\mathbf{k}$ is so-called Wannier function. Here Ω' is the Brillouin Zone, i.e., the unit cell in $\mathbf{k}$ plane. From the definition, one has that $w_{m,n}(\mathbf{r}) = w_{0,0}(\mathbf{r} - R_{m,n})$ where $R_{m,n} = m\mathbf{v}_1 + n\mathbf{v}_2$ denotes the position of the cell with indices (m, n). Sometimes the subscripts are omitted the Wannier function are

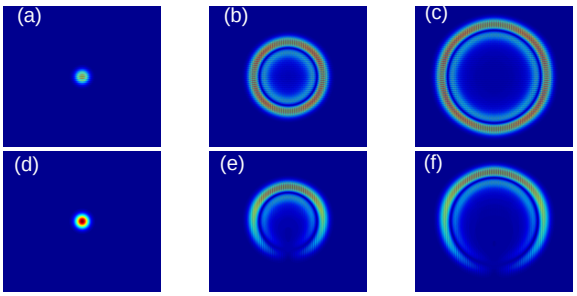

FIG. 2: The propagation of Bloch modes associated with a diabolical point; (a)-(c) two plane waves; (d)-(f) one plane wave: each is multiplied by a Gaussian envelope.

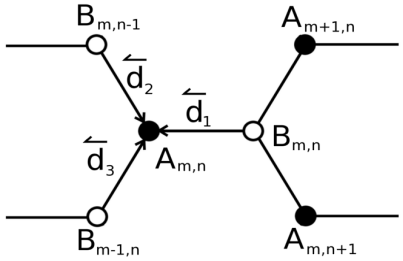

FIG. 3: The construction of the A and B lattices.

referred to as $w(\mathbf{r}-R_{m,n})$ which for large V_0 is localized and centered around $R_{m,n}$ for special values of $\mathbf{k}$.

Since μ is also periodic in $\mathbf{k}$ plane, one can also represent it as a Fourier series,

$$\mu(\mathbf{k}) = \sum_{m,n} \mu_{m,n} e^{-im\mathbf{k}\cdot\mathbf{v}_1 - in\mathbf{k}\cdot\mathbf{v}_2}. \tag{8}$$

Due to the properties of Wannier functions, any solution of equation (1) has the form

$$\psi(\mathbf{r},z) = \sum_{m,n,\alpha} C_{m,n,\alpha}(z) w_\alpha(\mathbf{r}-R_{m,n}) e^{-i\mathbf{k}\cdot R_{m,n}}. \tag{9}$$

Here $R_{m,n}$ stands for the position of unit cell with indices (m,n) and α is the index of different bands. In this paper, we only deal with the cases under which the components of higher bands are small, so only the first band expansion will be used. Thus, we discard the summation over α.

The above discussion is valid for any 2-D periodic lattice. However, the lattices we are dealing with in this paper are honeycomb lattices which have certain unique features. A key feature of a honeycomb lattice is that it contains two minima (sites A and B, dot and circle in Fig. 1 respectively) in the unit cell. In tight binding approximations, the honeycomb lattice can be broken up into two triangular sublattices: A and B lattices. In this case near a diabolical point, due to the degeneracy of the honeycomb lattice, the expansion (9) can be written in the form

$$\begin{aligned}\psi(\mathbf{r},z) &= \sum_{m,n} a_{m,n}(z)\tilde{w}(\mathbf{r}-A_{m,n})e^{-i\mathbf{k}\cdot A_{m,n}} \\ &+ \sum_{m,n} b_{m,n}(z)\tilde{w}(\mathbf{r}-B_{m,n})e^{-i\mathbf{k}\cdot B_{m,n}}.\end{aligned} \tag{10}$$

Here $A_{m,n}$ and $B_{m,n}$ are the site positions of the sublattices and $\tilde{w}(\mathbf{r})$ is the Wannier function associated with either of the triangular sublattices; it is localized and centered around the origin. The difference of two sublattices is just a spatial shift $a(1,0)$. The Wannier functions of two sublattices, determined by the local properties around the sites of the potential, are the same. Here $A_{m,n} = A_{0,0} + m\mathbf{v}_1 + n\mathbf{v}_2$, $B_{m,n} = B_{0,0} + m\mathbf{v}_1 + n\mathbf{v}_2$. We define three useful vectors, $\mathbf{d}_1 = A_{m,n} - B_{m,n} = a(-1,0)$, $\mathbf{d}_2 = A_{m,n} - B_{m,n-1} = a(\frac{1}{2}, -\frac{\sqrt{3}}{2})$ and $\mathbf{d}_3 = A_{m,n} - B_{m-1,n} = a(\frac{1}{2}, \frac{\sqrt{3}}{2})$. The vectors and their relations are shown in Fig. 3.

Substituting equations (9) and (8) into the lattice equation (1), we get

$$\begin{aligned}\sum_{m,n}\Big(& i\frac{da_{m,n}}{dz}S_A(m,n) + i\frac{db_{m,n}}{dz}S_B(m,n) \\ & - \sum_{m',n'} \mu_{m',n'} a_{m-m',n-n'} S_A(m-m',n-n') \\ & - \sum_{m',n'} \mu_{m',n'} b_{m-m',n-n'} S_B(m-m',n-n')\Big) \\ + & \Big(\sum_{m,n} a_{m,n}S_A(m,n) + b_{m,n}S_B(m,n)\Big)^2 \\ \times & \Big(\sum_{m,n} a_{m,n}S_A(m,n) + b_{m,n}S_B(m,n)\Big)^* \\ = & \ 0,\end{aligned} \tag{11}$$

where, for convenience, we introduce the notation $S_A(m,n) = \tilde{w}(\mathbf{r}-A_{m,n})e^{-i\mathbf{k}\cdot A_{m,n}}$ and $S_B(m,n) = \tilde{w}(\mathbf{r}-B_{m,n})e^{-i\mathbf{k}\cdot B_{m,n}}$.

We can reduce equation (11) to an explicit discrete equation. We assume $|\mu_{0,0}| \gg |\mu_{m,n}|, m \neq 0$ or $n \neq 0$. This assumption is valid when the intensity of the potential is large, (i.e. $V_0 >> 1$); i.e. the tight binding approximation. The tight binding approximation also relates Bloch functions to highly localized "Wannier functions" (cf. [10] for the tight binding approximation associated with the one-dimensional NLS lattice equation). Then we can neglect long-range interaction terms in the linear part of equation (11) and only consider nearest neighbors. In this context, multiply equation (11) by a specific $S_A^*(\bar{m},\bar{n})$(we drop the bar below) and integrate over whole $\mathbf{r}$ plane and introduce ϵ defined as

$$\epsilon = \frac{\int \tilde{w}^*(\mathbf{r}-A_{m,n})\tilde{w}(\mathbf{r}-B_{m,n})d\mathbf{r}}{\int |\tilde{w}(\mathbf{r}-A_{m,n})|^2 d\mathbf{r}}. \tag{12}$$

Notice that $w(\mathbf{r}-A_{m,n})$ is localized around $A_{m,n}$, so ϵ is small and, due to the properties of Wannier functions, is also independent

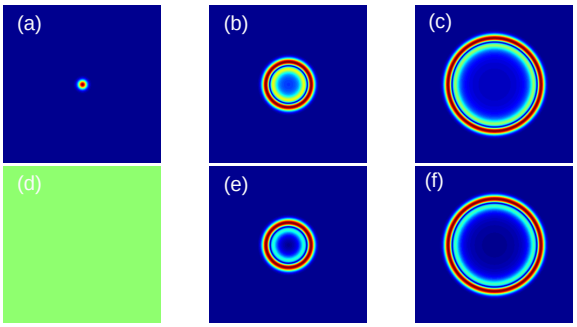

FIG. 4: Simulations of the Dirac equations (19-20) with $\sigma = 0$. The initial conditions are that a is a Gaussian and b is zero. (a)-(c) intensities of the a component at time 0, 5.4 and 10.8; (d)-(f) intensity of the b component at time 0, 5.4 and 10.8.

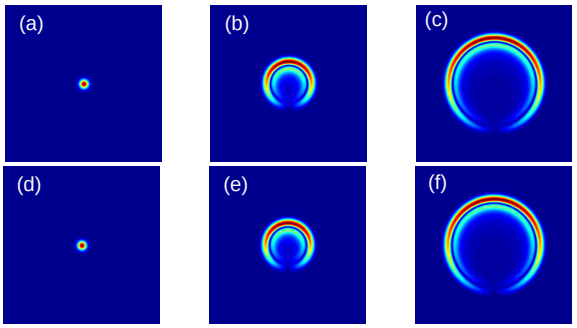

FIG. 5: Simulations of Dirac equations (19-20) with $\sigma = 0$. The initial conditions here are that a and b are the same Gaussian. (a)-(c) depict intensities of the a component at time 0, 5.4 and 10.8; and (d)-(f) the b component at time 0, 5.4 and 10.8.

of (m,n). Then $\frac{\int \tilde{w}^*(\mathbf{r}-A_{m,n})\tilde{w}(\mathbf{r}-B_{m-1,n})d\mathbf{r}}{\int |\tilde{w}(\mathbf{r}-A_{m,n})|^2 d\mathbf{r}}$ and $\frac{\int \tilde{w}^*(\mathbf{r}-A_{m,n})\tilde{w}(\mathbf{r}-B_{m,n-1})d\mathbf{r}}{\int |\tilde{w}(\mathbf{r}-A_{m,n})|^2 d\mathbf{r}}$ are also small and are both equal to ϵ. We also assume $\mu_{0,0}\epsilon = O(1)$, which leads to a maximally balanced equation.

Keeping the dominant terms, we get

$$i\frac{da_{m,n}}{dz} - \mu_{0,0}a_{m,n} + g\sigma|a_{m,n}|^2 a_{m,n} - \epsilon\mu_{0,0} \times(b_{m-1,n}e^{i\mathbf{k}\cdot\mathbf{d}_3} + b_{m,n-1}e^{i\mathbf{k}\cdot\mathbf{d}_2} + b_{m,n}e^{i\mathbf{k}\cdot\mathbf{d}_1}) = 0. \quad (13)$$

where $\mathbf{d}_i$ are defined below equation (10) and $g = \frac{\int |\tilde{w}(\mathbf{r}-A_{m,n})|^4 d\mathbf{r}}{\int |\tilde{w}(\mathbf{r}-A_{m,n})|^2 d\mathbf{r}}$ which is also independent of (m,n); similarly, we can get

$$i\frac{db_{m,n}}{dz} - \mu_{0,0}b_{m,n} + g\sigma|b_{m,n}|^2 b_{m,n} + \epsilon\mu_{0,0} \times(a_{m+1,n}e^{-i\mathbf{k}\cdot\mathbf{d}_3} + a_{m,n+1}e^{-i\mathbf{k}\cdot\mathbf{d}_2} + a_{m,n}e^{-i\mathbf{k}\cdot\mathbf{d}_1}) = 0. \quad (14)$$

Here we are studying the propagation of light beam with wave number $\mathbf{k}$ which is in the vicinity of diabolical points in the honeycomb lattice. The $\mathbf{k}$ in above analysis is one of the diabolical points. We choose $\mathbf{k} = K = (0, \frac{4\pi}{\sqrt{3}a})$.

Then we get the discrete equations

$$i\frac{da_{m,n}}{dz} - \mu_{0,0}a_{m,n} + g\sigma|a_{m,n}|^2 a_{m,n} - \epsilon\mu_{0,0} \times(b_{m-1,n}(-\frac{1}{2} + \frac{\sqrt{3}}{2}i) + b_{m,n-1}(-\frac{1}{2} - \frac{\sqrt{3}}{2}i) + b_{m,n}) = 0. \quad (15)$$

and

$$i\frac{db_{m,n}}{dz} - \mu_{0,0}b_{m,n} + g\sigma|b_{m,n}|^2 b_{m,n} - \epsilon\mu_{0,0} \times(a_{m+1,n}(-\frac{1}{2} - \frac{\sqrt{3}}{2}i) + a_{m,n+1}(-\frac{1}{2} + \frac{\sqrt{3}}{2}i) + a_{m,n}) = 0. \quad (16)$$

The system of equations (15) and (16) is the discrete Dirac system. In this paper we focus on the continuous problem. Taking the continuum limit of the discrete Dirac system, after some straightforward calculations, we obtain the governing equation

$$i\frac{\partial a}{\partial z} - \mu_{0,0}a - \frac{\sqrt{3}}{2}\epsilon\mu_{0,0}(\partial_x b - i\partial_y b) + g\sigma|a|^2 a = 0; \quad (17)$$

similarly, the b equation has the form

$$i\frac{\partial b}{\partial z} - \mu_{0,0}b + \frac{\sqrt{3}}{2}\epsilon\mu_{0,0}(\partial_x a + i\partial_y a) + g\sigma|b|^2 b = 0. \quad (18)$$

Notice that $\mu_{0,0}a$ and $\mu_{0,0}b$ can be absorbed into the first terms by defining new variables $\tilde{a} = ae^{-i\mu_{0,0}z}$ and $\tilde{b} = be^{-i\mu_{0,0}z}$(we drop the tildes below). Letting $D = -\frac{\sqrt{3}}{2}\epsilon\mu_{0,0}$ we finally get the continuous nonlinear Dirac system

$$i\frac{\partial a}{\partial z} + D(\partial_- b) + g\sigma|a|^2 a = 0; \quad (19)$$

$$i\frac{\partial b}{\partial z} - D(\partial_+ a) + g\sigma|b|^2 b = 0. \quad (20)$$

where $\partial_\pm = \partial_x \pm i\partial_y$.

Thus the evolution of envelopes of Bloch modes associated with the lattice NLS equation near a diabolical point are governed, in general, by a nonlinear Dirac system. If $\sigma = 0$, one gets linear Dirac system; but if $\sigma \neq 0$, we have a nonlinear Dirac system. Let us consider the linear system first. The dispersion relation for the linear system is defined by the equation

$$\begin{pmatrix} -\omega & D(ik_x + k_y) \\ D(-ik_x + k_y) & -\omega \end{pmatrix} \begin{pmatrix} \hat{a} \\ \hat{b} \end{pmatrix} = \begin{pmatrix} 0 \\ 0 \end{pmatrix}, \quad (21)$$

so the dispersion relation is

$$\omega^2 = D^2(k_x^2 + k_y^2). \quad (22)$$

This is a cone and this cone is exactly the dispersion relation of the honeycomb lattice near the diabolical point $K = (0, \frac{4\pi}{\sqrt{3}a})$.

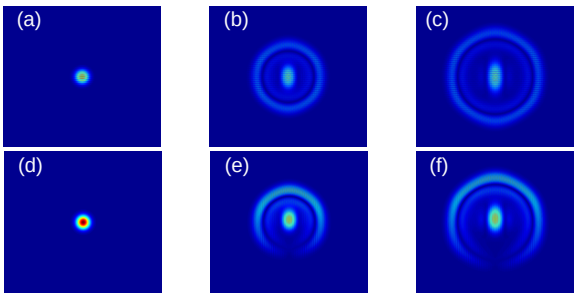

FIG. 6: The propagation of light beams in a saturable-type lattice –see eq. (25); (a)-(c) two plane waves; (d)-(f) one plane wave, each multiplied by a Gaussian envelope

The envelopes of the Bloch modes near diabolical point K disperse conically in the honeycomb lattices. This phenomenon can be described by the Dirac system (19)-(20). We know that there are two sets of opposite diabolical points which are equivalent to K and K'. The above derivation is for $K = (0, \frac{4\pi}{\sqrt{3}a})$. If we choose the other diabolical point $K' = (0, \frac{8\pi}{\sqrt{3}a})$, the analysis is exactly the same as well as the dispersion relation. However, the corresponding system becomes

$$i\frac{da}{dz} + D(\partial_+ b) + g\sigma|a|^2 a = 0; \tag{23}$$

$$i\frac{db}{dz} - D(\partial_- a) + g\sigma|b|^2 b = 0. \tag{24}$$

The only difference is just a variable change, $y \to -y$.

The two initial conditions in our direct lattice equation simulations are respectively: (1) both the a and b components are Gaussian; (2) the a component is a Gaussian while b is zero. In Fig. 2, we simulated the linear lattice NLS equations; i.e. $\sigma = 0$. So the corresponding Dirac system is linear. We simulate the linear Dirac system with these two sets of initial conditions. The results are displayed in Fig. 4 and Fig. 5. In Fig. 4, a is a unit Gaussian and b is zero initially. The intensities of both a and b are two perfect rings and the width of the rings doesn't change. This is consistent with the conical diffraction phenomenon which we observed in Fig. 2 (top row) and Preleg et. al observed in their experiments. On the other hand in Fig. 5, both a and b initially are unit Gaussians. The intensities of a and b have different ring structures from before in Fig. 4. Now the rings have notches at the bottom which correspond to the "half turn polarization" which we observed in direct lattice NLS equation simulations (see Fig. 2(bottom row)).

In order to compare our analysis with previous studies [9], we also simulated the saturable lattice equation:

$$i\psi_z + \nabla^2\psi + \frac{E_0}{1 + V(\mathbf{r}) + \sigma|\psi|^2}\psi = 0. \tag{25}$$

where $V(\mathbf{r})$ has the form in (2). In this case, we choose $\sigma = 0$, $V_0 = 0$ and $E_0 = 1000$. Launching two different initial beams, we get two evolution patterns which are displayed in Fig. 6. The evolution patterns are similar to the patterns in Fig. 2 except there is a central spot with saturable potential. Peleg et al. claimed that the central spot comes from higher band components which does not disperse conically [9]. The above analysis can be applied to the equation (25) and (apart from coefficient values) a Dirac system will be obtained. Hence one expects and finds that the main features in the evolution of the envelopes in both a linear potential lattice and the saturable potential lattice are similar since they are governed by the Dirac system. Details will be further investigated in the future.

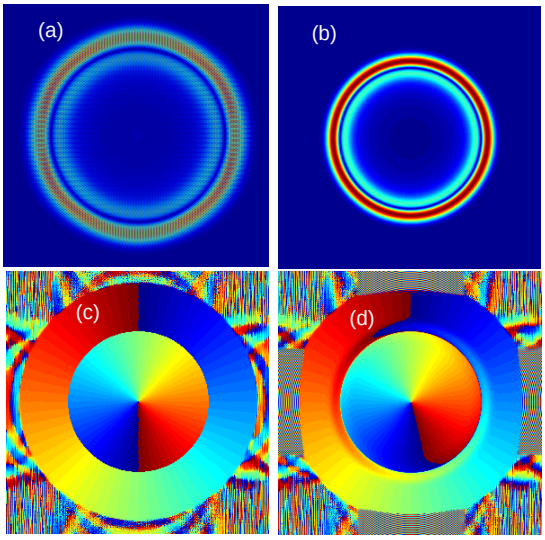

FIG. 7: Simulations of the nonlinear lattice equation (a) and the nonlinear Dirac system (b). The comparison of the phases in the simulations of both linear (c) and nonlinear (d) Dirac systems.

From the simulations and analysis, we obtained conical diffraction associated with the linear lattice. However we also note that the essentials of conical diffraction also exists in the presence of the lattice nonlinearity. We simulate the original lattice equation (1) with $\sigma = 1$ and find that the evolution of the intensities are almost the same as the linear case where $\sigma = 0$. A typical pattern is displayed in Fig. 7(a) which is corresponding to Fig. 2(c). We also simulate the nonlinear Dirac system we derived above, and the evolution of the intensities are almost the same as the linear case too. A typical pattern is displayed in Fig. 7(b)(nonlinear) which can be compared with Fig. 4(c) (linear). So conical diffraction does not only exist in the linear regime; but it is a nonlinear phenomena as well. The nonlinear Dirac system properly describes this phenomena. While the evolution of the intensities for both linear and nonlinear Dirac systems are essentially unchanged, the phases in linear and nonlinear systems are different (see Fig. 7(c)-(d)). A detailed analysis is outside the scope of this paper.

In summary, conical diffraction in honeycomb lattices was analyzed. In the tight binding limit, a discrete and

continuous Dirac system of evolution equations for the envelopes of two sublattice Bloch modes near diabolical points was derived. This Dirac system yields the same evolution patterns as in lattice NLS equations. Thus the tight binding limit contains the underlying mechanism of conical diffraction in honeycomb lattices. It is also found that conical diffraction survives in the presence of nonlinearity.

The authors thank Dr. Omri Bahat-Treidel, Dr. Or Peleg and Professor Jianke Yang for useful suggestions. This research was partially supported by the U.S. Air Force Office of Scientific Research, under grant FA4955-06-1-0237 and by the National Science Foundation, under grant DMS-0505352.

[1] W. R. Hamilton, "Third Supplement to an Essay on the Theory of Systems of Rays", Royal Irish Acad. , **17**, 1(1837).

[2] H. Lloyd, "On the phenomena presented by light in its passage along the axes of biaxial crystals", Trans. R. Ir. Acad., **17**, 145(1837).

[3] M. V. Berry and M. R. Jeffrey, "Conical diffraction: Hamilton's diabolical point at the heart of crystal optics", Progress in Optics, **50**, 13(2007).

[4] L. H. Haddad and L. C. Carr, "The Nonlinear Dirac Equation in Bose-Einstein Condensates: Foundation and Symmetries", Physica D, in press (2009).

[5] P.R. Wallace, "The Band Theory of Graphite", Physical Review, **71**, 622(1947).

[6] K. S. Novoselov *et al.*, Science **306**, 666(2004).

[7] O. Bahat-Treidel,*et al.*,"Symmetry Breaking in Honeycomb Photonic Lattices" Optics Lett. **33**, 2251 (2008).

[8] N.K. Efremidis *et al.*,"Two-Dimenional Optical Lattice Solitons" Phys. Rev. Lett. **91**, 213906 (2003).

[9] O. Peleg *et al.*,"Conical diffraction and gap solitons in honeycomb photonic lattices" Phys. Rev. Lett. **98**, 103901 (2007).

[10] G. L. Alfimov *et al.*,"Wannier functions analysis of the nonlinear Schrödinger equation with a periodic potential" Phys. Rev. E **66**, 046608 (2002).